NANO LETTERS

pubs.acs.org/NanoLett Letter

Confined Monolayer Ag As a Large Gap 2D Semiconductor and Its Momentum Resolved Excited States

Woojoo Lee, Yuanxi Wang, Wei Qin, Hyunsue Kim, Mengke Liu, T. Nathan Nunley, Bin Fang, Rinu Maniyara, Chengye Dong, Joshua A. Robinson, Vincent H. Crespi, Xiaoqin Li, Allan H. MacDonald, and Chih-Kang Shih*

Cite This: *Nano Lett.* 2022, 22, 7841−7847 Read Online

ACCESS | Metrics & More | Article Recommendations | Supporting Information

ABSTRACT: 2D materials have intriguing quantum phenomena that are distinctively different from their bulk counterparts. Recently, epitaxially synthesized wafer-scale 2D metals, composed of elemental atoms, are attracting attention not only for their potential applications but also for exotic quantum effects such as superconductivity. By mapping momentum-resolved electronic states using time-resolved and angle-resolved photoemission spectroscopy (ARPES), we reveal that monolayer Ag confined between bilayer graphene and SiC is a large gap (>1 eV) 2D semiconductor, consistent with ab initio GW calculations. The measured valence band dispersion matches the GW quasiparticle band structure. However, the conduction band dispersion shows an anomalously large effective mass of 2.4 m_0. Possible mechanisms for this large enhancement in the "apparent mass" are discussed.

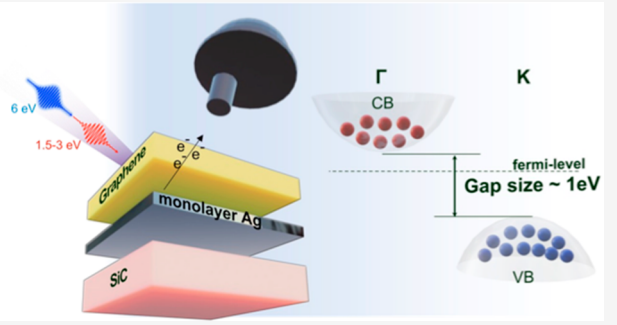

KEYWORDS: *2D metals, monolayer Ag, electronic structure, ultrafast photoemission spectroscopy, ARPES*

The capability to synthesize materials with atomic layer precision has enabled many scientific discoveries and advanced technologies, exemplified by the discovery of graphene and its derivatives.[1−4] Epitaxial metal layers have also inspired the discovery of several novel quantum effects in the ultrathin regime[5−8] although their investigations are often limited to ultrahigh-vacuum environments unless the surface is properly protected and stabilized by a capping layer.[9] Recently, a novel intercalation method was developed in which confined metal layers can be realized between a SiC substrate and a bilayer graphene (BL-Gr) capping layer which prevents oxidation of the confined epitaxial metals.[10,11] Intriguingly, such a confined metal layer may harbor novel electronic properties.[12,13] For example, density functional theory (DFT) predicted that silver- and indium-monolayer (MLs) are narrow-gap semiconductors due to their hybridization with the underlying SiC.[14] Indeed, recent ARPES investigations of the intercalated Ag monolayer (Ag-ML) revealed the existence of a valence band maximum (VBM) below the Fermi level.[15] However, the lack of information on the electronic structure above the Fermi level has impeded this new platform to be utilized in science and technology. One of the reasons for detaining its investigation is that the conventional alkali doping method does not work effectively for graphene-based systems.[16] The Schottky contact between the semiconducting Ag-ML and the metallic graphene makes it difficult to tune the Fermi level above the conduction band minimum (CBM) using alkali doping, thus preventing the excited states from being accessed using static-ARPES.

Here, we report ARPES and time-resolved ARPES (trARPES) investigations of the electronic structures of both occupied and unoccupied states in the confined Ag-ML between a SiC substrate and BL-Gr. We find that the confined Ag-ML is indeed an artificial 2D semiconductor with a surprisingly large bandgap (∼1 eV). Theory predicts this bandgap correctly when quasiparticle effects are accounted for (without the inclusion of graphene layer) using GW calculations on top of mean-field DFT results. The valence band dispersion is found to be consistent between the experiment and DFT+GW calculations. However, the conduction band dispersions differ substantially. The experimental effective mass is found to be a factor of 2.6 larger than the theoretical prediction. Moreover, the energy at the $\bar{M}_{Ag}$ point is revealed to be only 0.14 eV higher than the CBM at the Γ point, in stark contrast to a predicted value of 0.6 eV in DFT+GW calculations. These unusual features are attributed

Received: June 24, 2022
Revised: September 8, 2022
Published: September 20, 2022

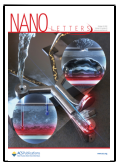

https://doi.org/10.1021/acs.nanolett.2c02501
Nano Lett. 2022, 22, 7841−7847

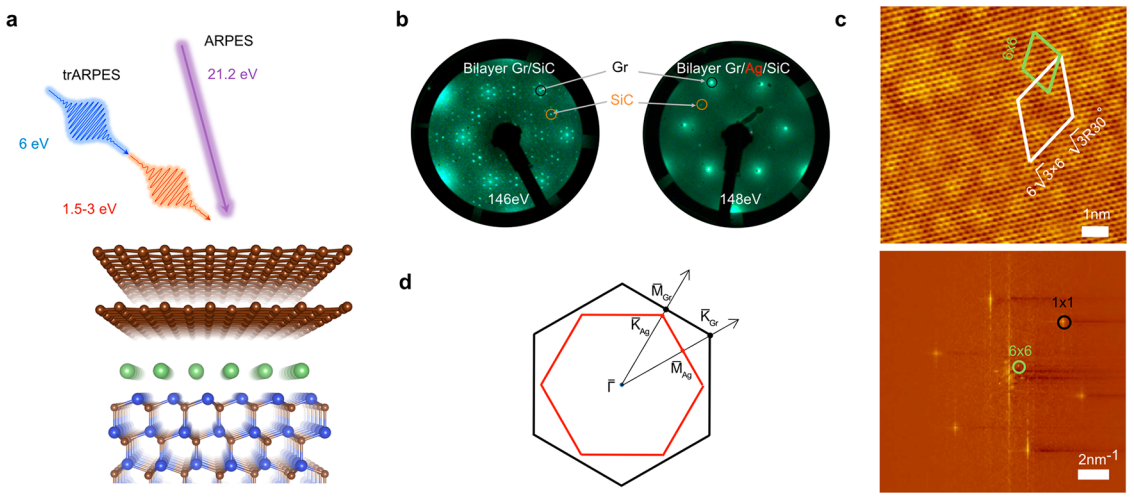

Figure 1. Monolayer Ag atomic structure and surface characterization. (a) Experimental scheme and atomic structure of intercalated Ag between bilayer graphene and SiC. (b) Low energy electron diffraction (LEED) images before and after Ag intercalation. (c) STM topography (top) and its real space fast Fourier transform (FFT) image (bottom). (d) Brillouin zones of monolayer Ag (red) and bilayer graphene (black).

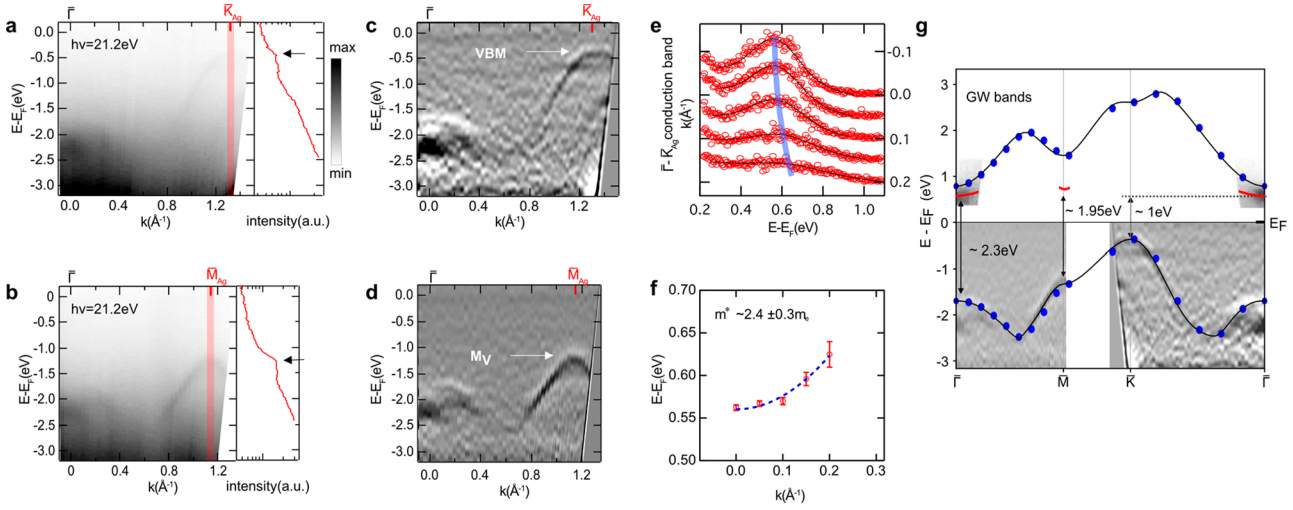

Figure 2. Occupied and unoccupied electronic structures of monolayer Ag. (a, b) Occupied band dispersions along high symmetry directions. (c, d) Second derivative images of a and b, respectively. (e) Unoccupied structure of the monolayer Ag along the $\bar{\Gamma}-\bar{K}_{Ag}$ direction. (f) The conduction band's effective mass determined from EDC fittings. (g) GW quasiparticle band structure superimposed with acquired experimental images. The experimental conduction band dispersion near the $\bar{\Gamma}$ point (up to $k_{\parallel} = 0.2$ Å^{-1}) is marked by a red curve. The energy location at the $\bar{M}_{Ag}$ point is marked by a red bar.

to the results of excitonic effect by precluding many-body interactions between the highly n-doped BL-Gr and Ag-ML electrons.

The atomic structure of the confined metal monolayer and the experimental setup are illustrated in Figure 1a. At the thermodynamic ground state, the Ag-ML assumes the lattice constant of SiC with surface Ag atoms projecting vertically onto the second topmost layer of C sites in the SiC substrate; the next most stable Ag registry (Ag projecting onto the *topmost* C sites) is higher in energy by +8 meV per Ag. Here we focus on the ground state structure, since other thermodynamically competing structures can be ruled out by comparing electronic structures with experiment (see Computational Details in Methods). The BL-Gr protects the confined epitaxial Ag from oxidation, allowing sample transport under ambient conditions. The confined growth of metal monolayers using epitaxial graphene as a template has been described previously.[10] The same procedure is used in this study to intercalate Ag atoms between the BL-Gr and SiC substrate. All samples were cleaned in the ultrahigh-vacuum (UHV) chamber (pressure <1 × 10^{-10} mbar) by overnight annealing at 220 °C. A thoroughly cleaned sample exhibits a sharp graphene 1 × 1 LEED pattern coexisting with another pattern consistent with the SiC lattice constant (Figure 1b). The commonly observed sharp $6\sqrt{3} \times 6\sqrt{3}R30°$ patterns for pristine BL-Gr on SiC become a fuzzy ring, suggesting a decoupling of BL-Gr and SiC due to Ag intercalation. STM studies, however, still exhibit a quasi 6 × 6 superstructure superimposed on the graphene 1 × 1 lattice (Figure 1c), consistent with the Ag-ML following the SiC lattice constant.[15] Based on this structural information, the surface Brillouin zones (BZs) for BL-Gr and Ag-ML are determined in Figure 1d.

The occupied band dispersions of Ag-ML are obtained along two major directions, $\bar{\Gamma}-\bar{K}_{Ag}$ and $\bar{\Gamma}-\bar{M}_{Ag}$. The static-ARPES data using 21.2 eV photon energy is shown in Figure 2a and b,

https://doi.org/10.1021/acs.nanolett.2c02501
Nano Lett. 2022, 22, 7841−7847

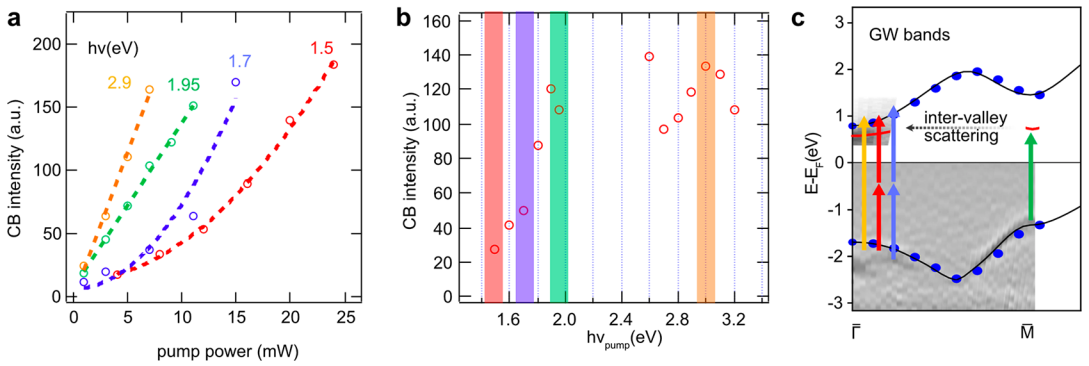

Figure 3. Below-bandgap absorption at $\bar{M}_{Ag}$ point. (a) Pump power dependence of $\bar{\Gamma}$ point CB intensity at four pump photon energies. Linear (1.95 and 2.9 eV) and quadratic (1.5 and 1.7 eV) dispersions reflect one-photon absorption (1PA) and two-photon absorption (2PA) processes. (b) CB intensity versus pump photon energy at fixed 4 mW pump power (85 μJ/cm^2). (c) Schematic of 1PA and 2PA process at $\bar{M}_{Ag}$ and $\bar{\Gamma}$ points. The smaller photon energies, $h\nu_{pump}$ < 1.95 eV, excite the electrons to $\bar{\Gamma}$ point CB via 2PA. On the other hand, at a higher photon energy, $h\nu_{pump}$ = 1.95 eV, the system absorbs the photons via 1PA by forming the quasi-particle bound states (excitons) which are immediately scattered to $\bar{\Gamma}$, resulting in the hot exciton dispersion.

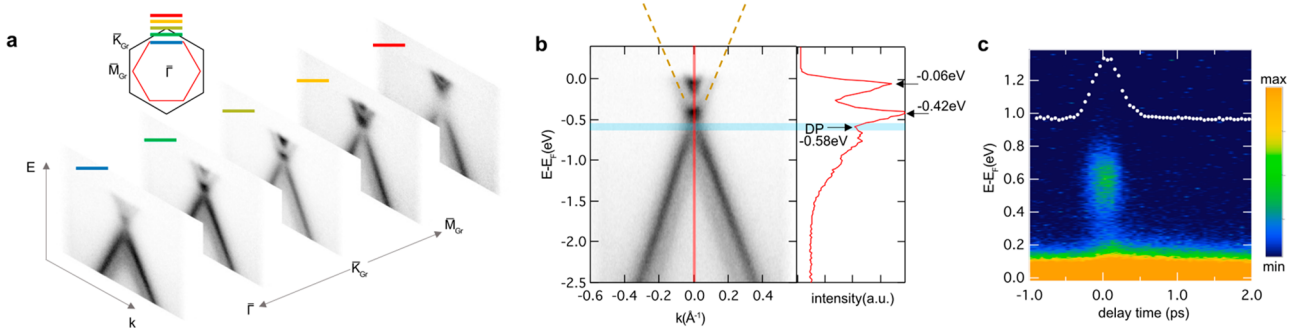

Figure 4. High electron density in the bilayer graphene and an ultrafast decay of the Ag monolayer's CB state. (a) Dirac cone dispersions along the $\bar{\Gamma}$–$\bar{K}_{Gr}$ direction. (b) Zoomed-in Dirac cone at the $\bar{K}_{Gr}$ point. (c) Photoelectron intensity versus energy and time delay at the $\bar{\Gamma}$ point. White dots indicate the CBM intensity distribution.

respectively, and their second-derivative counterparts are shown in Figure 2c and d. The valence band maximum (VBM) is identified at $\bar{K}_{Ag}$ with a binding energy of ∼0.45 eV below E_F. At the saddle point $\bar{M}_{Ag}$, a local maximum is identified as $\bar{M}_V \sim -1.25$ eV. Near the $\bar{\Gamma}$ point, the SiC band structure is also observed with SiC_{VBM} located around −1.8 eV. The same band dispersion with different photon energy (40.8 eV) can be found in Figure S1. We note that our VB mapping result is very similar to that reported recently for Ag-ML confined between ML-Gr and SiC,[15] except for the absolute energy relative to the Fermi level.

Next, we reveal the unoccupied band dispersion near $\bar{\Gamma}$ using trARPES with 3 eV photons (Figure 2e). A color-coded spectra image can be found in Figure S2. The CBM is identified at ∼0.56 eV above E_F, and its peak position does not show probe power dependence, indicating the absence of the space charge effect (Figure S3). Moreover, the possibility that this state is induced by imaging potential or multibands is ruled out by performing pump photon energy-dependent measurements (Figure S4) and by reported DFT calculations on Ag-ML/SiC[14] combined with experimental observations of BL-Gr CB bands.[17] The effective mass, 2.4 ± 0.3 m_0, of the conduction band is determined by mapping the dispersion from $k_{\|}$ = 0 to $k_{\|}$ = 0.2 Å^{-1} (Figure 2f). The acquired occupied/unoccupied band dispersions reveal an indirect gap of 1.01 eV, a value significantly larger than the earlier DFT prediction of 0.2 eV.[14]

To better capture this large bandgap feature, we carried out GW corrections on top of DFT calculations (see details in Methods) and superimposed the results on the experimental observation as shown in Figure 2g. To make the DFT+GW calculations computationally feasible, the graphene cap is excluded, which simplifies the computation cell to a minimal SiC surface unit cell. The calculation predicts a bandgap value of ∼1.15 eV, consistent with the experimental observation. Moreover, the valence band dispersion from the DFT+GW calculations agrees well with the experimental results. The difference (0.15 eV) between the experimental and the calculated bandgap sizes may be attributed to dielectric/Coulomb screening from graphene layers, which was not explicitly included in the GW calculations. Such a renormalization effect on graphitic substrates[18−22] has been intensively studied recently.

By contrast, the calculated conduction band dispersion clearly differs from the experimental observation. The GW quasiparticle band dispersion near CBM yields an effective mass of 0.94 m_0, a factor of 2.6 lighter than the experimental estimate. Moreover, as discussed further below, the GW calculation predicts that the $\bar{M}_{Ag}$ point gap size is ∼2.63 eV after considering the −0.15 eV error, thus a strong light absorption is expected at the same size of photon energy. However, the absorption was observed at 1.95 eV.

To gain further insight, we performed trARPES as a function of the pump photon energy. Figure 3a shows the photoelectron intensity near the CBM as a function of pump power for four

https://doi.org/10.1021/acs.nanolett.2c02501
Nano Lett. 2022, 22, 7841−7847

different pump photon energies. The quadratic dependence on the pump power clearly shows two-photon absorption (2PA) processes for $h\nu$ = 1.5 and 1.7 eV. On the other hand, for $h\nu$ = 1.95 and 2.9 eV, only the one-photon absorption (1PA) event is involved as revealed by the linear dependence. Figure 3b shows the photoelectron intensity near the CBM vs pump energy at a constant incident pump fluence of ∼85 μJ/cm^2. The plot shows that as the $h\nu_{pump}$ drops below 1.95 eV, the excitation efficiency to the conduction band quickly decreases, consistent with the existence of a threshold of $h\nu \approx$ 1.95 eV for a transition from a 2PA to a 1PA process.

As the direct gap at the $\bar{\Gamma}$ point is ∼2.35 eV, it is not surprising that excitations to the CB using $h\nu$ = 1.5 and 1.7 eV require 2PA (and for that matter, 1PA for $h\nu \approx$ 2.9 eV; see Figure 3c). What is surprising is that only 1PA is involved for $h\nu \approx$ 1.95 eV, which is smaller than the direct gap at the $\bar{\Gamma}$ and $\bar{M}_{Ag}$ points. This unexpected observation leads us to consider two possible origins of the observed large effective mass at the $\bar{\Gamma}$-point: a band renormalization by an interaction between plasmons on BL-Gr and electrons on Ag-ML and an exciton-dressed band dispersion. An alternative mechanism for the 1.95 eV threshold for the single photon process entails the excitation of hot carriers in the graphene layer, which is then transferred to the Ag-ML conduction band. Our analysis, however, suggests that the contribution from this alternative process would be less likely (Supplementary Note 1).

We first characterize the high electron density in the BL-Gr embodying collective modes of electrons (plasmon) and discuss its role in the Ag-ML's electronic system. Shown in Figure 4a are E vs k mappings for a series of k-space segments perpendicular to the $\bar{\Gamma}-\bar{K}_{Gr}$ direction. The zoomed-in image of the band mapping at $\bar{K}_{Gr}$ is shown in Figure 4b. One can see a gap opening at the Dirac point (DP) due to the lattice symmetry breaking along the c-axis creating a vertical electric field.[23,24] The splitting between the coupled Dirac bands in BL-Gr is observable with two Fermi wavevectors, $k_{F,1}$ = 0.11 ± 0.01 Å^{-1} and $k_{F,2}$ = 0.03 ± 0.01 Å^{-1}. The energy separation for the two Dirac bands above the DP is ∼0.36 eV. The Fermi velocity v_F, fitted at $k_{F,1}$, is 0.55 × 10^6 cm/s, about half of the Dirac velocity of the unperturbed Dirac cone in single-layer graphene. The Dirac electron density, n_s, is related to the Fermi wavevector by $n_s = k_F^2/\pi$, from which we calculate an electron density of ∼4 × 10^{13}/cm^2. The BL-Gr electronic structure is consistent with previously reported results for the same density.[16]

Given the high electron density in the BL-Gr, plasmons can be generated[25,26] and interact with electrons[27] in the Ag-ML. The electron−plasmon interactions are expected to renormalize electron effective mass analogous to electron−phonon interactions.[28] For quantitative analysis, we model and solve a Hamiltonian to get an interaction-induced self-energy and a renormalized mass of electrons in the Ag-ML. The detailed derivation can be found in Supplementary Note 2. Despite the existence of finite mass enhancement, the result shows that it is less than 2% of the free electron mass. We attribute this inefficient enhancement to the much faster dynamics of plasmons than Ag electrons as represented in their dispersive band (Supplementary Figure S6). Within the time scale of the Ag electron dynamics, the contributions from the plasmon modes are averaged to negligible value. This is in analogy to the electron−electron interaction-dressed electron effective mass. Although the Coulomb interaction is strong, its effect on electron effective mass is very weak and can be ignored. Thus, we conclude that the mass enhancement driven by electron-plasmon interaction cannot provide a satisfactory explanation for our experimental results. On the other hand, the ultrafast decay time of the excited state implies that the electron-plasmon coupling still plays an important role as an efficient energy relaxation channel (Figure 4c).

We next discuss an excitonic effect on the acquired band dispersion. The exciton, a quasi-particle commonly observed in 2D semiconductors, consists of an electron−hole pair attracted via Coulomb interaction. This two-particle bound state can participate in the photoemission process by leaving the hole behind the escaped electron. The escaped electron states are expected to have a downward-parabolic dispersion in energy-momentum (E-k) space as governed by energy conservation law.[29] On the other hand, at finite temperature, the ensemble of thermally excited hot exciton states modifies the parabolic dispersion to be opened upward, mimicking a single-electron dispersion but with a heavier effective mass, $m_e + m_h$.[29] To this end, we presume the exciton-dressed band dispersion as an origin of the experimentally determined large effective mass, 2.4 ± 0.3 m_0.

Considering the exciton-dressed band dispersion, it is intriguing that the 1PA, at photon energies smaller than the direct gap at the $\bar{\Gamma}$ and $\bar{M}_{Ag}$ points, led to populate the CB states. According to the DFT+GW calculations, the $\bar{M}_{Ag}$ point is a saddle point in the E-k dispersion for both CB and VB, resulting in a diverging density of states. Thus, the 1PA threshold of 1.95 eV can be interpreted as the excitonic transition. Given the $\bar{M}_{Ag}$ point gap size of ∼2.63 eV, it implies an exciton binding energy of ∼0.68 eV, which is consistent with binding energies observed in various 2D semiconductors.[30] Once the excitons are formed, it is expected to be scattered transiently to the $\bar{\Gamma}$ point exciton state via intervalley exciton scattering by leaving electrons at the $\bar{\Gamma}$ valley and holes at the $\bar{K}_{Ag}$ valley, i.e., momentum-forbidden dark excitons. The intervalley exciton scattering was observed directly in monolayer WSe_2 and MoS_2 by photoemission experiments.[31,32] We expect that the same effect is manifested here. Unfortunately, in the current case, the CB state's lifetime is much shorter than our time resolution, precluding us from observing the dynamical behavior of excitons as reported for WSe_2 and MoS_2 monolayers.[31,32]

In summary, we combined ARPES and trARPES to probe momentum-resolved quasi-particle dispersions for both the equilibrium and excited states and revealed that a confined Ag monolayer between SiC and BL-Gr is an artificial 2D semiconductor with an indirect band gap of 1 eV. We also showed that the equilibrium quasi-particle dispersion in the valence band dispersion is well-captured by the DFT+GW calculation. However, the excited state dispersion in the conduction band is dramatically different, exemplified by an anomalously large effective mass (a factor of 2.6 enhancement). We attribute this massive enhancement to the consequence of exciton-dressed band dispersion by precluding another scenario, mass enhancement induced by electron-plasmon interactions, which only contribute to the rapid decay time.

METHODS

Sample Preparation. Epitaxial graphene (EG) is synthesized via sublimation of silicon from the (0001) plane of semi-insulating 6H-SiC (II−VI Inc.) at 1800 °C, 700 Torr pressure, and 500 sccm Ar flow, for 30 min. EG is then plasma treated

https://doi.org/10.1021/acs.nanolett.2c02501
Nano Lett. 2022, 22, 7841−7847

using a Tepla M4L plasma etch tool, using 150 sccm of O_2 and 50 sccm of He, under a pressure of 500 mTorr and power of 50W for 60 s. Two-dimensional silver intercalation was performed using a Thermo Scientific Lindberg/Blue M Mini-Mite tube furnace fitted with a 1-in. outer diameter quartz tube. A custom-made alumina crucible from Robocasting Enterprises was used to hold 1 × 1 cm EG/SiC substrates. The EG grown face is placed downward inside the crucible. Then, 75 mg of silver powder (Sigma-Aldrich, 99.999%) was placed in the crucible directly beneath the EG/SiC substrate. The crucible with EG/SiC and the silver powder was then loaded into the tube furnace and evacuated to ∼5 mTorr. The tube was then pressurized to 500 Torr with Ar. The furnace was then heated to 950 °C with a ramp rate of 50° min^{-1} and an Ar flow of 50 sccm. The furnace was held at the growth temperature for 1 h, then cooled to room temperature.

Experimental Details. *ARPES/6 eV-trARPES Measurements.* A Scienta R3000 hemisphere analyzer was used to collect the photoemission spectra for both static-ARPES and 6 eV-trARPES measurements. The static ARPES measurements were carried out with a helium lamp using He I-α (21.2 eV) and He II-α (40.8 eV). During the helium lamp measurements, the pressure was better than 6 × 10^{-10} Torr. The 6 eV-trARPES measurements were performed using probe pulse (206 nm) and pump pulse (826−387 nm). The pressure was maintained below 8 × 10^{-11} Torr. The fundamental 1030 nm pulses from a carbide laser of light conversion were used for the fifth harmonic generator (HIRO) and Orpheus-HP optical parametric amplifier (OPA) to generate the pump and probe pulses at a 100 kHz repetition rate. All measurements were performed at room temperature. The pump−probe cross-correlation width was estimated as 400 fs (fwhm) via the fastest photoemission dynamics. The incident fluence was ∼85 $\mu J/cm^2$.

Computational Details. DFT+GW calculations were based on the Ag/SiC structure described in the main text. Additional DFT calculations were performed for structures with Ag projecting onto the topmost C sites and onto the topmost Si sites, where M point energies were 0.47 and 0.80 eV relative to the CBM, respectively, neither smaller than that of the main Ag/SiC structure we considered of 0.45 eV. This excludes the possibility that the small M point energy could be due to a thermodynamically competing Ag surface phase. In all DFT+GW calculations, we employ an 18 × 18 × 1 k-point grid and a truncated Coulomb interaction.[33] We employ the extrapolar technique[34] to achieve convergence for all quasiparticle band energies within 0.05 eV. Extrapolar energy of 2.0 Ha was extracted from systematic convergence studies, allowing accelerated convergence at a plane-wave energy cutoff of 10 Ha and 100 empty bands for the evaluation of the dielectric matrix and self-energies. The calculated static dielectric matrix was extended to finite frequencies using the Godby−Needs-generalized plasmon-pole model.[35] All calculations are performed using the ABINIT code.[36]

■ ASSOCIATED CONTENT

Data Availability Statement

The data that support the findings of this study are available from the corresponding author upon reasonable request.

Supporting Information

The Supporting Information is available free of charge at https://pubs.acs.org/doi/10.1021/acs.nanolett.2c02501.

Gr/Ag/SiC electronic band structure acquired with 40.8 eV photon energy, color-coded CB spectra of monolayer Ag, 6 eV probe pulse power dependence at CBM, pump photon energy dependence at CBM, charge transfer from bilayer graphene, and electron-plasmon interaction-induced mass renormalization (PDF)

■ AUTHOR INFORMATION

Corresponding Author

Chih-Kang Shih − *Department of Physics, The University of Texas at Austin, Austin, Texas 78712, United States; Center for Dynamics and Control of Materials, The University of Texas at Austin, Austin, Texas 78712, United States;* orcid.org/0000-0003-2734-7023; Email: shih@physics.utexas.edu

Authors

Woojoo Lee − *Department of Physics, The University of Texas at Austin, Austin, Texas 78712, United States; Center for Dynamics and Control of Materials, The University of Texas at Austin, Austin, Texas 78712, United States;* orcid.org/0000-0003-4705-6522

Yuanxi Wang − *Two-Dimensional Crystal Consortium and Materials Research Institute, The Pennsylvania State University, University Park, Pennsylvania 16802, United States; Department of Physics, University of North Texas, Denton, Texas 76203, United States*

Wei Qin − *Department of Physics, The University of Texas at Austin, Austin, Texas 78712, United States; Center for Dynamics and Control of Materials, The University of Texas at Austin, Austin, Texas 78712, United States*

Hyunsue Kim − *Department of Physics, The University of Texas at Austin, Austin, Texas 78712, United States; Center for Dynamics and Control of Materials, The University of Texas at Austin, Austin, Texas 78712, United States*

Mengke Liu − *Department of Physics, The University of Texas at Austin, Austin, Texas 78712, United States; Center for Dynamics and Control of Materials, The University of Texas at Austin, Austin, Texas 78712, United States*

T. Nathan Nunley − *Department of Physics, The University of Texas at Austin, Austin, Texas 78712, United States; Center for Dynamics and Control of Materials, The University of Texas at Austin, Austin, Texas 78712, United States*

Bin Fang − *Center for Dynamics and Control of Materials, The University of Texas at Austin, Austin, Texas 78712, United States*

Rinu Maniyara − *Materials Science and Engineering, The Pennsylvania State University, University Park, Pennsylvania 16802, United States*

Chengye Dong − *Two-Dimensional Crystal Consortium and Materials Research Institute, The Pennsylvania State University, University Park, Pennsylvania 16802, United States*

Joshua A. Robinson − *Two-Dimensional Crystal Consortium and Materials Research Institute, The Pennsylvania State University, University Park, Pennsylvania 16802, United States; Materials Science and Engineering, The Pennsylvania State University, University Park, Pennsylvania 16802, United States;* orcid.org/0000-0002-1513-7187

Vincent H. Crespi − *Two-Dimensional Crystal Consortium and Materials Research Institute, The Pennsylvania State University, University Park, Pennsylvania 16802, United States; Department of Physics, The Pennsylvania State*

https://doi.org/10.1021/acs.nanolett.2c02501
Nano Lett. 2022, 22, 7841−7847

University, University Park, Pennsylvania 16802, United States

Xiaoqin Li − *Department of Physics, The University of Texas at Austin, Austin, Texas 78712, United States; Center for Dynamics and Control of Materials, The University of Texas at Austin, Austin, Texas 78712, United States*

Allan H. MacDonald − *Department of Physics, The University of Texas at Austin, Austin, Texas 78712, United States; Center for Dynamics and Control of Materials, The University of Texas at Austin, Austin, Texas 78712, United States*

Complete contact information is available at: https://pubs.acs.org/10.1021/acs.nanolett.2c02501

Author Contributions

W.L., J.A.R., and C.K.S. conceived the experiment. W.L. carried out trARPES/ARPES measurements. Y.W. and V.C. performed DFT-GW calculations. R.M., C.D., and J.A.R. prepared the sample. M.L. performed STM measurements. W.L. created a platform for 6 eV trARPES and UHV investigation with the participation of H.K., T.N.N., and B.F. under the joint supervision of C.K.S. and X.L. A.H.M. and W.Q. performed theoretical model calculations. W.L., C.K.S., and A.H.M analyzed the data. W.L. and C.K.S. wrote the manuscript with substantial contributions from all of the authors.

Notes

The authors declare no competing financial interest.

■ ACKNOWLEDGMENTS

This work was primarily supported by the National Science Foundation through the Center for Dynamics and Control of Materials: an NSF MRSEC under Cooperative Agreement No. DMR-1720595. Other support includes NSF Grant Nos. DMR-1808751 and the Welch Foundation F-1672. Support for synthesis comes from The Penn State Center for Nanoscale Science (NSF Grant DMR-2011839) and the Penn State 2DCC-MIP (NSF DMR-1539916).

■ REFERENCES

(1) Novoselov, K. S.; Geim, A. K.; Morozov, S. V.; Jiang, D.; Katsnelson, M. I.; Grigorieva, I. V.; Dubonos, S. V.; Firsov, A. A. Two-Dimensional Gas of Massless Dirac Fermions in Graphene. *Nature* **2005**, *438* (7065), 197−200.

(2) Zhang, Y.; Tan, Y.-W.; Stormer, H. L.; Kim, P. Experimental Observation of the Quantum Hall Effect and Berry's Phase in Graphene. *Nature* **2005**, *438* (7065), 201−204.

(3) Mak, K. F.; Lee, C.; Hone, J.; Shan, J.; Heinz, T. F. Atomically Thin MoS2: A New Direct-Gap Semiconductor. *Phys. Rev. Lett.* **2010**, *105* (13), 136805.

(4) Splendiani, A.; Sun, L.; Zhang, Y.; Li, T.; Kim, J.; Chim, C.-Y.; Galli, G.; Wang, F. Emerging Photoluminescence in Monolayer MoS2. *Nano Lett.* **2010**, *10* (4), 1271−1275.

(5) Qin, S.; Kim, J.; Niu, Q.; Shih, C.-K. Superconductivity at the Two-Dimensional Limit. *Science* **2009**, *324* (5932), 1314−1317.

(6) Chiang, T.-C. Photoemission Studies of Quantum Well States in Thin Films. *Surf. Sci. Rep.* **2000**, *39* (7), 181−235.

(7) Lu, Y.-J.; et al. Plasmonic Nanolaser Using Epitaxially Grown Silver Film. *Science* **2012**, *337* (6093), 450−453.

(8) Himpsel, F. J.; Ortega, J. E.; Mankey, G. J.; Willis, R. F. Magnetic Nanostructures. *Adv. Phys.* **1998**, *47* (4), 511−597.

(9) Nam, H.; et al. Ultrathin Two-Dimensional Superconductivity with Strong Spin-Orbit Coupling. *Proc. Natl. Acad. Sci. U. S. A.* **2016**, *113* (38), 10513−10517.

(10) Briggs, N.; Gebeyehu, Z. M.; Vera, A.; Zhao, T.; Wang, K.; De La Fuente Duran, A.; Bersch, B.; Bowen, T.; Knappenberger, K. L.; Robinson, J. A. Epitaxial Graphene/Silicon Carbide Intercalation: A Minireview on Graphene Modulation and Unique 2D Materials. *Nanoscale* **2019**, *11* (33), 15440.

(11) Briggs, N.; et al. Atomically Thin Half-van Der Waals Metals Enabled by Confinement Heteroepitaxy. *Nat. Mater.* **2020**, *19* (6), 637−643.

(12) Hsu, C.-H.; Lin, W.-H.; Ozolins, V.; Chuang, F.-C. Electronic Structures of an Epitaxial Graphene Monolayer on SiC(0001) after Metal Intercalation (Metal = Al, Ag, Au, Pt, and Pd): A First-Principles Study. *Appl. Phys. Lett.* **2012**, *100* (6), 063115.

(13) Forti, S.; Link, S.; Stöhr, A.; Niu, Y.; Zakharov, A. A.; Coletti, C.; Starke, U. Semiconductor to Metal Transition in Two-Dimensional Gold and Its van Der Waals Heterostack with Graphene. *Nat. Commun.* **2020**, *11* (1), 2236.

(14) Wang, Y.; Crespi, V. H. Atlas of 2D Metals Epitaxial to SiC: Filling-Controlled Gapping Conditions and Alloying Rules. *arXiv* **2020**, 10.48550/arXiv.2011.01914.

(15) Rosenzweig, P.; Starke, U. Large-Area Synthesis of a Semiconducting Silver Monolayer via Intercalation of Epitaxial Graphene. *Phys. Rev. B* **2020**, *101* (20), 201407.

(16) Rosenzweig, P.; Karakachian, H.; Marchenko, D.; Starke, U. Surface Charge-Transfer Doping a Quantum-Confined Silver Monolayer beneath Epitaxial Graphene. *Phys. Rev. B* **2022**, *105* (23), 235428.

(17) Jobst, J.; Kautz, J.; Geelen, D.; Tromp, R. M.; van der Molen, S. J. Nanoscale Measurements of Unoccupied Band Dispersion in Few-Layer Graphene. *Nat. Commun.* **2015**, *6* (1), 8926.

(18) Ugeda, M. M.; et al. Giant Bandgap Renormalization and Excitonic Effects in a Monolayer Transition Metal Dichalcogenide Semiconductor. *Nat. Mater.* **2014**, *13* (12), 1091−1095.

(19) Utama, M. I. B.; et al. Dielectric-Defined Lateral Heterojunction in a Monolayer Semiconductor. *Nat. Electron* **2019**, *2* (2), 60−65.

(20) Raja, A.; Chaves, A.; Yu, J.; Arefe, G.; Hill, H. M.; Rigosi, A. F.; Berkelbach, T. C.; Nagler, P.; Schuller, C.; Korn, T.; Nuckolls, C.; Hone, J.; Brus, L. E.; Heinz, T. F.; Reichman, D. R.; Chernikov, A.; et al. Coulomb Engineering of the Bandgap and Excitons in Two-Dimensional Materials. *Nat. Commun.* **2017**, *8*, 15251.

(21) Waldecker, L.; et al. Rigid Band Shifts in Two-Dimensional Semiconductors through External Dielectric Screening. *Phys. Rev. Lett.* **2019**, *123* (20), 206403.

(22) Steinke, C.; Wehling, T. O.; Rösner, M. Coulomb-Engineered Heterojunctions and Dynamical Screening in Transition Metal Dichalcogenide Monolayers. *Phys. Rev. B* **2020**, *102* (11), 115111.

(23) Ohta, T.; Bostwick, A.; Seyller, T.; Horn, K.; Rotenberg, E. Controlling the Electronic Structure of Bilayer Graphene. *Science* **2006**, *313* (5789), 951−954.

(24) McCann, E.; Fal'ko, V. I. Landau-Level Degeneracy and Quantum Hall Effect in a Graphite Bilayer. *Phys. Rev. Lett.* **2006**, *96* (8), 086805.

(25) Borghi, G.; Polini, M.; Asgari, R.; MacDonald, A. H. Dynamical Response Functions and Collective Modes of Bilayer Graphene. *Phys. Rev. B* **2009**, *80* (24), 241402.

(26) Sensarma, R.; Hwang, E. H.; Das Sarma, S. Dynamic Screening and Low-Energy Collective Modes in Bilayer Graphene. *Phys. Rev. B* **2010**, *82* (19), 195428.

(27) Overhauser, A. W. Simplified Theory of Electron Correlations in Metals. *Phys. Rev. B* **1971**, *3* (6), 1888−1898.

(28) Grimvall, G. *The Electron-Phonon Interaction in Metals*; North-Holland: Amsterdam, 1981.

(29) Rustagi, A.; Kemper, A. F. Photoemission Signature of Excitons. *Phys. Rev. B* **2018**, *97* (23), 235310.

(30) Mueller, T.; Malic, E. Exciton Physics and Device Application of Two-Dimensional Transition Metal Dichalcogenide Semiconductors. *npj 2D Mater. Appl.* **2018**, *2* (1), 1−12.

(31) Madéo, J.; et al. Directly Visualizing the Momentum-Forbidden Dark Excitons and Their Dynamics in Atomically Thin Semiconductors. *Science* **2020**, *370* (6521), 1199−1204.
(32) Lee, W.; Lin, Y.; Lu, L.-S.; Chueh, W.-C.; Liu, M.; Li, X.; Chang, W.-H.; Kaindl, R. A.; Shih, C.-K. Time-Resolved ARPES Determination of a Quasi-Particle Band Gap and Hot Electron Dynamics in Monolayer MoS2. *Nano Lett.* **2021**, *21* (17), 7363−7370.
(33) Ismail-Beigi, S. Truncation of Periodic Image Interactions for Confined Systems. *Phys. Rev. B* **2006**, *73* (23), 233103.
(34) Bruneval, F.; Gonze, X. Accurate G W Self-Energies in a Plane-Wave Basis Using Only a Few Empty States: Towards Large Systems. *Phys. Rev. B* **2008**, *78* (8), 085125.
(35) Godby, R. W.; Needs, R. J. Metal-Insulator Transition in Kohn-Sham Theory and Quasiparticle Theory. *Phys. Rev. Lett.* **1989**, *62* (10), 1169−1172.
(36) Gonze, X.; et al. ABINIT: First-Principles Approach to Material and Nanosystem Properties. *Comput. Phys. Commun.* **2009**, *180* (12), 2582−2615.

https://doi.org/10.1021/acs.nanolett.2c02501
Nano Lett. 2022, 22, 7841−7847